Applied Catalysis B: Environmental 199 (2016) 372–383

Contents lists available at ScienceDirect

Applied Catalysis B: Environmental

journal homepage: www.elsevier.com/locate/apcatb

$MgO/NiAl_2O_4$ as a new formulation of reforming catalysts: Tuning the surface properties for the enhanced partial oxidation of methane

Zouhair Boukha, Cristina Jiménez-González, Miryam Gil-Calvo, Beatriz de Rivas, Juan Ramón González-Velasco, Jose Ignacio Gutiérrez-Ortiz, Rubén López-Fonseca *

Chemical Technologies for Environmental Sustainability Group, Department of Chemical Engineering, Faculty of Science and Technology, University of The Basque Country UPV/EHU, P.O. Box 644, E-48080 Bilbao, Spain

ARTICLE INFO

Article history:
Received 6 May 2016
Received in revised form 13 June 2016
Accepted 18 June 2016
Available online 19 June 2016

Keywords:
Nickel aluminate
Magnesium oxide
Surface basicity
Partial oxidation of methane

ABSTRACT

Magnesia modified nickel aluminate spinel catalysts were synthesised and characterised by BET, TEM, XRD, H_2-TPR, XPS, CO_2-TPD and TGA-MS techniques. The addition of this promoter induced significant changes in the textural, structural and chemical properties of the resulting spinel derived catalysts. Thus, it enhanced the resistance of the deposited Ni particles against sintering, whereas, upon increasing MgO loading, it drastically modified the density and the strength of the surface basic sites. In fact, an apparent weakening of the surface basic sites with the abundance of highly dispersed Mg species was interestingly observed.

The changes provoked by MgO addition deeply influenced the catalytic performance of the prepared samples in the partial oxidation of methane reaction at 700 °C. In this sense, it was found a good correlation between the measured density of the strong basic sites on the different samples, including the bare $NiAl_2O_4$, and their catalytic activity. Hence, the MgO(5 wt.%)/$NiAl_2O_4$ sample, with a magnesium loading close to the theoretical monolayer and the lowest strong basic density sites, exhibited the best catalytic performance under both stoichiometric (O/C = 1) and non-stoichiometric (O/C = 0.75) conditions during a relatively prolonged time on stream.

1. Introduction

The application of energy technology based on hydrogen as energy vector is a promising alternative, to traditional fossil fuels combustions, which could facilitate the transition to a sustainable development of clean energy systems [1–3]. Nowadays, hydrogen is mostly produced *via* steam reforming of methane (SRM, Ec. (1)). Nevertheless, this process is relatively expensive due to its high endothermicity [4,5]. For this reason the partial oxidation of methane (POM, Ec. (2)) is often viewed as a more advantageous strategy since the process needs a lower energy input due to its mild exothermicity, which reduces operation costs. Thus, the technology does not need an external fired heater which makes it simpler and more practical for small reactors used in mobile applications [6–9]. Furthermore, the POM is a good option when the posterior use of the syngas stream requires a suitable H_2/CO ratio. Nevertheless, there are many parallel reactions that could occur during the POM process, such as water gas shift reaction (WGS, Ec. (3)) and/or methane total oxidation (Ec. (4)), which produce significant amounts of carbon dioxide in the product gas [10–12].

$$CH_4+H_2O \rightarrow 3H_2+CO \Delta H^{\circ}_{25^{\circ}C} = +206 kJ\ mol^{-1} \quad (1)$$

$$CH_4+0.5O_2 \rightarrow 2H_2+CO \Delta H^{\circ}_{25^{\circ}C} = -36 kJ\ mol^{-1} \quad (2)$$

$$CO+H_2O \rightarrow CO_2+H_2O \Delta H^{\circ}_{25^{\circ}C} = -41 kJ\ mol^{-1} \quad (3)$$

$$CH_4+2O_2 \rightarrow CO_2+2H_2O \Delta H^{\circ}_{25^{\circ}C} = -890 kJ\ mol^{-1} \quad (4)$$

It is known that noble metals, such as Rh and Pt, exhibit a good reforming activity and high resistance against carbon formation. However, this high cost limits their utilisation. As a result, research is extensively focused on other promising substitutes based on active transition metals [11,13–15]. Among the non-noble metals, Ni-based catalysts have similar activity compared to those based on noble metals [9,13,16,17]. Nevertheless, they are very sensitive to the structural changes that can affect their active species under the severe conditions of the preparation (reduction at high temperatures) and during the reforming catalytic process. According to many authors these changes may provoke decay in their activity and stability [16–22]. In this sense, many efforts have been devoted

* Corresponding author.
E-mail address: ruben.lopez@ehu.es (R. López-Fonseca).

http://dx.doi.org/10.1016/j.apcatb.2016.06.045
0926-3373/

to develop active and stable catalysts (minimizing sintering and coking) by optimising the preparation route to achieve high nickel dispersion. In this sense, the literature proposes some strategies based on the preparation of spinel (NiM_2O_4) [18,19] or perovskite ($MNiO_3$) [20–22] phases as catalyst precursors, where nickel is stabilised in a well-defined structure. For instance, in our previous studies we demonstrated that the $NiAl_2O_4$ spinel materials, reduced at high temperature (850 °C), led to a formation of metallic nickel supported on alumina surface with high dispersion and relatively small crystallite size [13,23]. These synthesised catalysts proved high activity, selectivity and stability in various methane reforming reactions, compared to those prepared by conventional routes.

Also, within the objective to improve activity and stability of Ni catalysts, by reducing the Ni crystallites sizes and their stabilisation against sintering, the effect of the addition of some alkali and alkaline earth metals used as chemical promoters has been extensively investigated [8,24–26]. For instance, Sousa et al. [27] studied the relationship between structure and deactivation in the dry reforming of methane over Ni/alumina doped with CeO_2, MgO, ZrO_2 and La_2O_3 catalysts. Their results showed that the catalyst promoted with MgO exhibited the highest performance amongst all the investigated materials. This behaviour was explained by a synergetic effect between nickel species and $MgAl_2O_4$/$NiAl_2O_4$ structures which enhanced the resistance to structural transformations and inhibited carbon formation. By contrast, Kirillov et al. [9] observed some structural changes on Ni/MgO/alumina catalysts used in partial oxidation of methane for 100 h, but this was not at the expense of their activity. Besides its promotional effect on the structural properties of Ni catalysts many investigations highlighted the suitable surface basicity provided by MgO promoter which greatly influences the adsorption-desorption of reaction intermediates and thus the catalytic reforming performance [28].

The major objective of this work is the analysis of textural, chemical and structural properties and catalytic behaviour of a set of nickel aluminate samples with varying the amount of MgO promoter. The choice of the magnesia loading in the 2.5–10 wt.% range has been made in accordance with the BET surface area of the prepared catalysts to obtain surface Mg densities ranging from submonolayer to over-monolayer values. It should be noted that, to our knowledge, the modification of $NiAl_2O_4$ spinel materials with MgO, their characterisation and their catalytic performance in the POM reaction have not been yet investigated. Special attention has been devoted to the influence of MgO loading on the physico-chemical and catalytic properties of the reduced MgO/$NiAl_2O_4$ samples.

2. Experimental

2.1. Catalysts preparation

Bulk $NiAl_2O_4$ (MgO(0)-NiAl sample) was synthesised from a mixture of two aqueous solutions $Ni(CH_3\text{-}COO)_2{\cdot}4H_2O$ and $Al(NO_3)_3{\cdot}9H_2O$, with the desired 1:2 Ni/Al molar ratio. The final pH of the aqueous solution was adjusted at 8 by adding aqueous ammonia (0.6 M). The precipitate was subsequently aged for 30 min before being filtered and washed with hot deionised water. Afterwards the recovered solid was dried at 110 °C overnight and then calcined at 850 °C in static air for 4 h at a heating rate of 10 °C min^{-1} [23].

The incorporation of magnesium oxide on the nickel aluminate (3 g) was carried out by wet impregnation with an aqueous solution of $Mg(NO_3)_2{\cdot}6H_2O$. The samples were dried at 110 °C overnight and then calcined at 850 °C in static air for 2 h using a heating rate of 10 °C min^{-1}. The catalysts were labelled MgO(2.5)-NiAl, MgO(5)-NiAl, MgO(7)-NiAl and MgO(10)-NiAl, which corresponded to MgO loadings of 2.5, 5, 7 and 10 wt.%, respectively. NiO and MgO pure oxides were prepared by simple calcination at 850 °C in air of nickel acetate and magnesium nitrate, respectively. Referring to the $MgAl_2O_4$ sample was obtained commercially from Sigma-Aldrich.

2.2. Catalyst characterisation

The catalysts were characterised by N_2 physisorption at −196 °C, wavelength dispersive X-ray fluorescence (WDXRF), X-ray diffraction (XRD), temperature programmed reduction with hydrogen (H_2-TPR), X-ray photoelectron spectroscopy (XPS), transmission electron microscopy (TEM) and temperature programmed desorption of CO_2 (CO_2-TPD). The experimental details of each analytical technique were described elsewhere [13,23].

Additionally, the surface basicity of the reduced samples was characterised by temperature programmed desorption of CO_2 techniques (CO_2-TPD). These studies were carried out on an experimental setup coupled to a MKS Cirrus LM99 mass spectrometer. Prior to running the TPD experiments, the oxide samples (200 mg) were submitted to a pre-treatment routine consisting of a reduction step at 850 °C (2 h) in a flow 5%H_2/Ar, cooling to 40 °C in a flow of He, treatment in a flow of CO_2/He for 1 h at 40 °C, and finally 1 h under flowing He, also at 40 °C. The thermo desorption of CO_2 step was carried out under He flow rate of 50 cm^3 min^{-1} and a heating ramp of 10 °C min^{-1} (up to 900 °C).

The spent samples were characterised by S_{BET} measurements, XRD, TEM and thermogravimetry coupled to mass spectrometry (TGA-MS).

2.3. Catalytic tests

Catalytic tests were performed in a bench-scale fixed-bed reactor (Microactivity modular laboratory system provided by PID Eng&Tech S.L) operated at atmospheric pressure and fully monitored by computer. The reactor was made of stainless steel with an internal diameter of 9 mm and a height of 305 mm, in which the temperature was controlled by a thermocouple placed in the catalyst bed. Typically 0.125 g of catalyst in powdered form (0.3–0.5 mm) was loaded. The catalysts bed was diluted with inert quartz 1:1 (1–1.25 mm). Different experiments were carried out to evaluate the catalytic activity and stability of the samples. Firstly, a feed gas mixture containing 10%CH_4, 5%O_2 (O/C = 1) and balanced with N_2 was used. Hence, a volume hourly space velocity at 38400 cm^3 CH_4 g^{-1} h^{-1} was maintained using Bronkhorst mass flow controllers. Before the reaction, the catalyst was reduced *in situ* under 5% H_2/N_2 at 850 °C for 2 h. The experiments were carried out at constant temperature (700 °C) for about 20 h.

The catalysts were also intentionally run under more severe conditions to allow meaningful reactivity and stability comparison. Thus, maintaining the same time on stream (20 h) and operation temperature (700 °C), the volume hourly space velocity at 60000 cm^3 CH_4 g^{-1} h^{-1} (15.6%CH_4/5.9%O_2/78.5%N_2) was increased while the O/C mole ratio was lowered down to 0.75. Additional experiments were conducted over a more prolonged time on line (75 h).

On basis of the dry molar flow at the inlet and outlet of the reactor, conversion and product yields were calculated, according to the following equations:

$$X(CH_4), \% = \frac{F_{out}(CO) + F_{out}(CO_2)}{F_{in}(CH_4)} \times 100 \quad (5)$$

$$Y(H_2) = \frac{F_{out}(H_2)}{2 \times F_{in}(CH_4)} \quad (6)$$

$$Y(CO) = \frac{F_{out}(CO)}{F_{in}(CH_4)} \quad (7)$$

Table 1
Elemental analysis and textural properties of the MgO(x)-NiAl catalysts.

Catalysts	Ni, wt.%[a]	MgO, wt.%[a]	S_{BET}, $m^2\ g^{-1}$	W_p, nm	V_p, $cm^3\ g^{-1}$
MgO(0)-NiAl	(32.1)	(0)	67 (75)	14.4 (12.7)	0.32 (0.30)
MgO(2.5)-NiAl	(31.5)	(2.4)	64 (68)	14.5 (12.9)	0.29 (0.29)
MgO(5)-NiAl	(31)	(4.9)	62 (62)	15 (13.8)	0.29 (0.28)
MgO(7)-NiAl	(30.4)	(7)	59 (61)	15.5 (13.9)	0.28 (0.28)
MgO(10)-NiAl	(29.7)	(10)	59 (59)	16.6 (15.4)	0.31 (0.28)

Values in brackets correspond to the calcined catalysts.
[a] Determined by WDXRF.

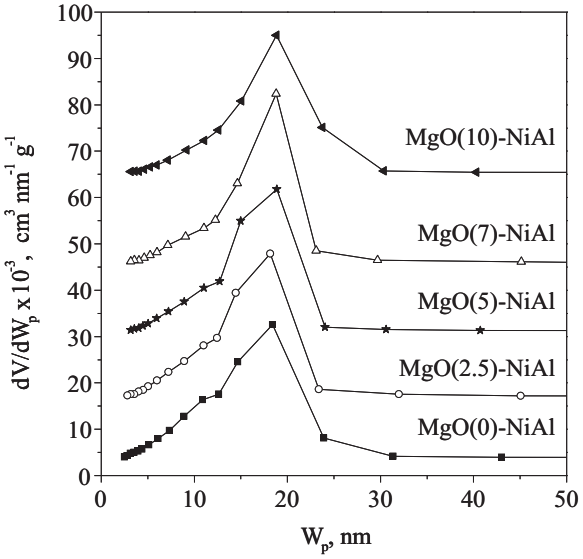

Fig. 1. Pore sizes distribution for the reduced MgO(x)-NiAl catalysts.

$$Y(CO_2) = \frac{F_{out}(CO_2)}{F_{in}(CH_4)} \quad (8)$$

3. Results and discussion

3.1. Characterisation of the fresh samples

3.1.1. N_2-physorption (BET measurements)

The textural properties of the calcined and reduced MgO(x)-NiAl catalysts were examined by nitrogen adsorption-desorption measurements. All the samples exhibited IV-type isotherms, indicating the existence of well-developed mesopores, with significantly reduced hysteresis loops (not shown). The corresponding specific surface area values are reported in Table 1. The magnesia unmodified catalyst (MgO(0)-NiAl) presented a specific surface area of 75 $m^2\ g^{-1}$. Upon addition of MgO the surface area significantly decreased. Hence, for MgO-rich samples it was 61 $m^2\ g^{-1}$ for MgO(7)-NiAl and 59 $m^2\ g^{-1}$ for MgO(10)-NiAl.

The reduction of the MgO(0)-NiAl catalyst provoked a significant drop (about 10%) in its specific surface area, from 75 to 67 $m^2\ g^{-1}$. However, this loss of surface area associated with the phase transformation from $NiAl_2O_4$ to Ni/Al_2O_3 was less evident in the presence of increased amounts of Mg. Thus, this resistance against the decrease of surface area was notably enhanced with MgO loading. For instance, the reduction of the sample with the highest MgO loading, MgO(10)-NiAl, did not affect its specific surface area (59 $m^2\ g^{-1}$).

Fig. 1 shows the pore size distributions of the reduced samples. The shape of the traces of the samples with a low MgO loading (≤5%) looked similar. Their distribution were, thus, characterised by a main peak centred at approximately 18 nm and a shoulder at 14 nm. However, for higher MgO loadings (≥7%) the pore sizes had a unimodal distribution located at 18 nm, thereby revealing the absence of narrower pores peak (at 14 nm). Since the surface density of Mg atoms in the MgO(5)-NiAl sample was 11.8 at. nm^{-2}, very close to the theoretical surface monolayer, 12.4 at. nm^{-2}, we might reasonably conclude that most of narrow pores of MgO-rich samples were completely filled by the over-monolayer Mg species.

3.1.2. X-ray diffraction (XRD)

The MgO(x)-NiAl samples were also characterised by means of X-ray powder diffraction in order to investigate the effect of the MgO addition on their structural properties. Fig. 2 compares the XRD patterns for all the prepared MgO(x)-NiAl in their calcined (850 °C) and reduced (850 °C) states (Fig. 2(a) and (b), respectively). The crystalline phases were identified using the JCPDS files. Expectedly the calcined MgO(0)-NiAl sample displayed a set of diffraction peaks centred at 2θ = 19.3°, 31.5°, 37.2°, 45.2°, 59.9° and 65.7°, assignable to the nickel aluminate phase (JCPS 78–1601) [29]. Furthermore, the MgO(0)-NiAl diffractogram showed additional peaks associated with NiO structure, at 43.6° and 62.9° (JCPDS 89–7131). It should be noted that the XRD patterns of the calcined MgO catalysts showed a significant evolution of the NiO diffraction peaks which shifted to lower angles. This effect was more pronounced on the MgO-rich samples. For instance, 2θ angle shifted from 43.6° for MgO(0)-NiAl sample to 43.5° and 43.4° for MgO(7)-NiAl and MgO(10)-NiAl, respectively. These observations suggested the diffusion of Mg^{2+} cations in NiO crystal lattice to form MgO-NiO solid solution [26]. Moreover, the slight shift might be explained by the identical structures of NiO and MgO phases and their very close lattice parameters.

Fig. 2(b) includes the diffractograms of the MgO(x)-NiAl catalysts after reduction at 850 °C. As expected, the MgO(0)-NiAl pattern showed a transformation of nickel aluminate and NiO structures into gamma alumina (JCPDS 79–1558) and metallic nickel (JCPDS 89–7128) phases. Apparently, no diffraction peaks associated with NiO or MgO were visible in the patterns of MgO(x)-NiAl catalysts. However, because of its high formation heat, above 420 kJ mol^{-1}, the reduction of magnesium oxide under the used reduction conditions (850 °C for 2 h) was ruled out. Then, the structural changes of Mg species provoked by the reduction process were followed by assessing the diffraction lines attributed to gamma alumina which seemed to shift to lower angles with MgO. Fig. 3 shows a correlation between the lattice parameter corresponding to gamma alumina structure and the Mg/Al molar ratios determined by WDXRF, for all the reduced samples and for pure $MgAl_2O_4$ used as reference. The results clearly indicated a shift of the lattice parameter (a) towards higher values with MgO loading, thereby suggesting a progressive formation of $MgAl_2O_4$. In their study on NiSn/MgO-Al_2O_3 materials Penkova et al. [30] attributed this shift to the formation of magnesium aluminate phase. In this sense Jacob et al. [31] also reported that the formation of $MgAl_2O_4$ from MgO and Al_2O_3 could start at around 800 °C.

The average size of Ni particles calculated by Scherrer equation was found to be around 11 nm on the MgO(0)-NiAl catalyst while somewhat smaller particles with an average size of about 9–9.5 nm were detected for the magnesia modified catalysts (Table 2). We

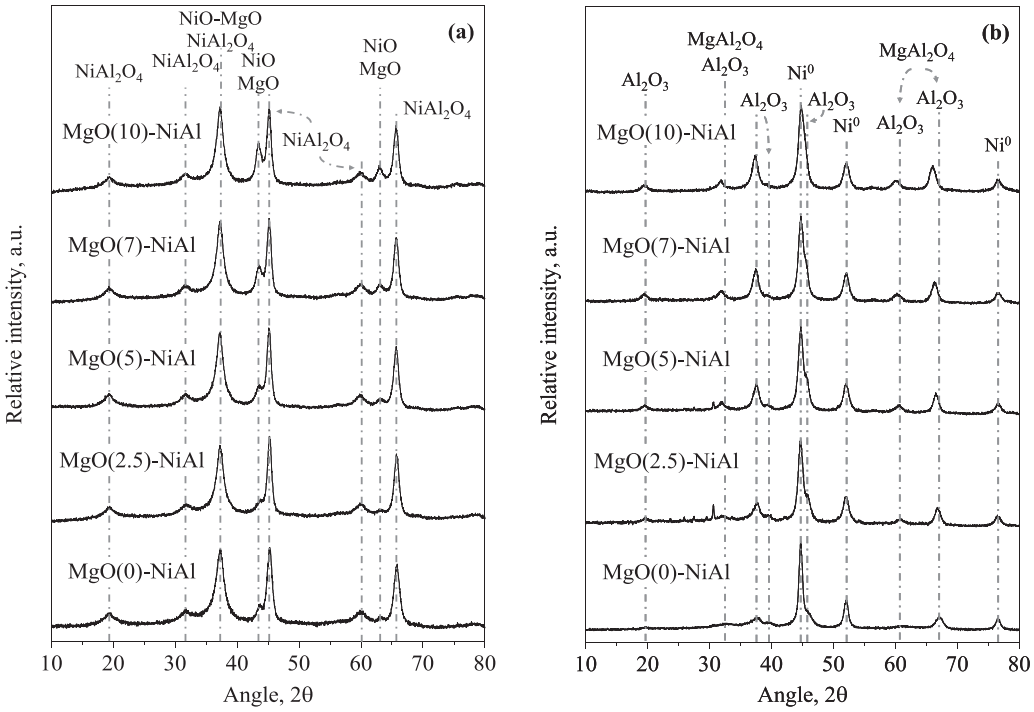

Fig. 2. XRD patterns of the (a) calcined and (b) reduced MgO(x)-NiAl catalysts.

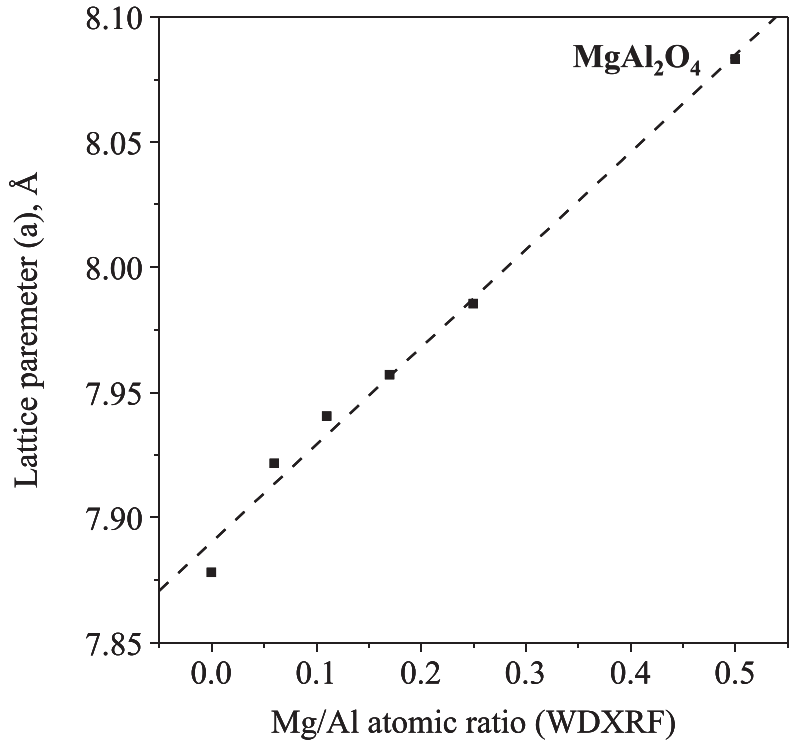

Fig. 3. Correlation between the lattice parameter corresponding to γ-alumina and the Mg/Al molar ratios as determined by WDXRF.

might conclude that the deposition of MgO enhanced the resistance against metallic nickel sintering.

3.1.3. Temperature programmed reduction (H_2-TPR)

The H_2-TPR experiments were performed in order to identify the various Ni reducible species and the influence of MgO on the reducibility of the calcined MgO(x)-NiAl samples (Fig. 4). It should be noted that no reduction peaks were detected on the H_2-TPR profiles of $MgAl_2O_4$ and MgO samples used as reference (not displayed). The H_2-TPR curve of MgO(0)-NiAl sample exhibited a typical profile of non-stoichiometric nickel aluminate materials. This exhibited three reduction peaks centred at 490, 720 and 805 °C. The former, α-type NiO, was attributed to the reduction of NiO species which had strong interaction with the spinel phase. The two high-temperature reduction peaks at 720 and 805 °C were associated with the reduction of the Ni^{2+} species incorporated in an

Table 2
Reducibility and structural properties of the MgO(x)-NiAl catalysts.

Catalysts	H_2 uptake, mmol g^{-1}	H_2-TPR					TEM			XRD (Ni^0 particle size, nm)		
		Relative amount of NiO species, %[a]				Reduction degree, %	Ni^0 particle size, nm	D, %[b]	S_{Ni}[c], m^2_{Ni} g^{-1}	Reduced catalysts	Spent catalysts[d]	Spent catalysts[e]
		α	β	γ	θ							
MgO(0)-NiAl	5.6	19 (490)	39 (720)	42 (805)	0	100	13	7.0	12	11	9.	18
MgO(2.5)-NiAl	5.6	22 (480)	40 (740)	38 (815)	0	100	11	8.9	15	9.5	13	14
MgO(5)-NiAl	5.1	25 (525)	40 (750)	35 (825)	0	100	11.5	8.7	15	9	12	13.5
MgO(7)-NiAl	5.2	12 (480)	59 (720)	25 (835)	4 (>860)	100	11	9.4	15	9	11	15
MgO(10)-NiAl	4.7	16 (505)	49 (715)	26 (860)	10 (>860)	94	11	8.7	14	9	9	13

[a] Values in brackets correspond to the peak temperature (°C) of each reduction band.
[b] Ni dispersion taking into account the extent of reduction at 850 °C.
[c] Metallic surface area taking into account the extent of reduction at 850 °C.
[d] Reaction conditions: 38400 cm^3 CH_4 g^{-1} h^{-1}; 10%CH_4/5%O_2/85%N_2; 700 °C; 20 h.
[e] Reaction conditions: 60000 cm^3 CH_4 g^{-1} h^{-1}; 15.6%CH_4/5.9%O_2/78.5%N_2; 700 °C; 20 h.

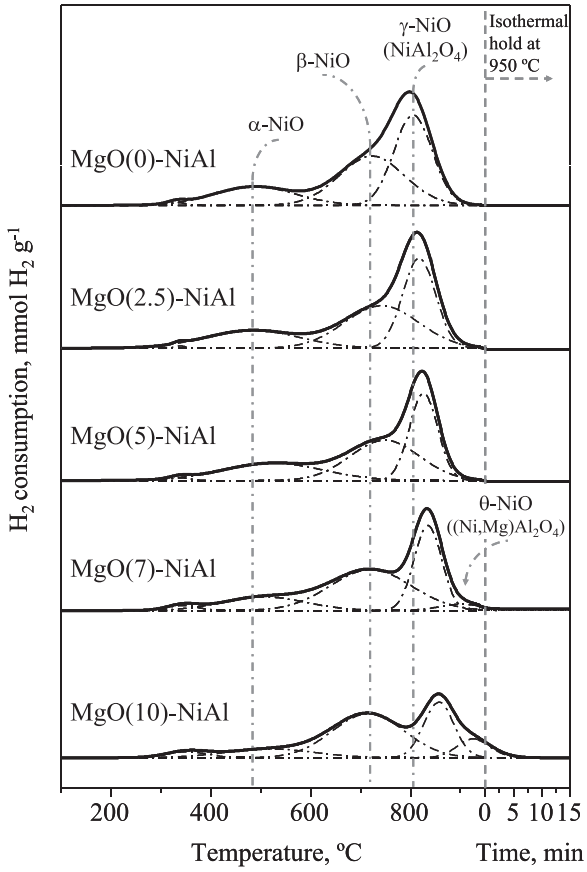

Fig. 4. H_2-TPR profiles of the calcined MgO(x)-NiAl catalysts.

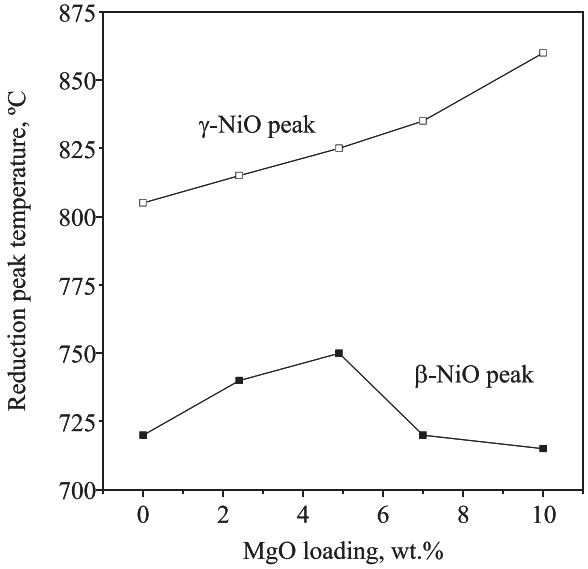

Fig. 5. Dependence of the reduction peak temperatures on the MgO loading for the MgO(x)-NiAl catalysts.

inverse nickel aluminate structure. In our previous study we proved that, in an inverse spinel structure, the Ni^{2+} ions located in octahedral sites (β-type NiO) were more prone to be reduced compared to these located in tetrahedral sites (γ-type NiO) [23].

Similar reduction traces were observed for MgO(x)-NiAl samples. Nevertheless, significant changes in the H_2-TPR peaks positions and their relative contribution could be noted. Table 2 summarises the H_2-TPR quantitative data extracted from the inte-

gration of the Ni reduction bands. The reduction degree was also calculated as the ratio between the measured H_2 uptake and theoretical H_2 amounts needed for a complete reduction of Ni^{2+} ions. The analysis of the obtained results suggested that the reduction of γ-type NiO species was strongly influenced by increased MgO amounts leading to higher reduction temperatures . For instance, it shifted from 805 °C for the MgO(0)-NiAl to 860 °C for the MgO(10)-NiAl catalyst. Furthermore, the progressive addition of magnesia led to a decrease of the contribution of γ-type NiO species (from 42% for MgO(0)-NiAl to 26% for MgO(10)-NiAl) (Table 2). It is also relevant to highlight that, at high temperatures (>860 °C), the MgO-rich catalysts exhibited additional reduction peaks which could be related to the reduction of Ni^{2+} in $(Mg,Ni)Al_2O_4$ mixed spinel [7,32]. This Ni species (θ-type NiO) represented 4% and 10% of the total Ni reducible species in the MgO(7)-NiAl and MgO(10)-NiAl samples, respectively. Regarding the effect of the addition of MgO on the reducibility of α-type and β-type NiO species, the highest reduction peak temperatures were found for the MgO(5)-NiAl catalyst, 525 °C for α-type NiO and 750 °C for β-type NiO (Fig. 5). As aforementioned this might be explained by a strong interaction of NiO with Mg species resulting from a surface density close to that corresponding to a theoretical surface monolayer.

3.1.4. X-ray photoelectron spectroscopy (XPS)

The surface chemical composition and the Ni and Mg structures lying on the surface of the MgO(x)-NiAl catalysts were investigated by means of XPS techniques. Fig. 6(a) displays the deconvoluted photoemission peaks for Ni $2p_{3/2}$ region. For all the analysed samples the main XPS peak located in the range 855–856 eV and the shake-up satellite peak in the range 861–862 eV showed that the Ni^{2+} ions were mainly incorporated in the network of $NiAl_2O_4$ structure [5,23,32]. However, as reported in Table 3, the XPS peak positions seemed to depend on the MgO content. For example, the MgO(5)-NiAl catalyst showed the lowest Ni $2p_{3/2}$ peak binding energy (855.2 eV). This shift was explained by an enrichment of the near surface of MgO(5)-NiAl sample with NiO [5,23]. Moreover, as revealed by the FWHM data reported in Table 3, the MgO(5)-NiAl sample showed the broadest Ni $2p_{3/2}$ peak (3.7 eV), thus suggesting a larger heterogeneity in nickel environments. These observations were in good agreement with the previously described H_2-TPR results which revealed that this sample exhibited, besides the $NiAl_2O_4$ phase, the highest amount of α-type NiO species. Furthermore, a parallel series of Mg 2p spectra was recorded for the MgO(x)-NiAl samples (Fig. 6(b)). The value of O 1 s level was taken as internal reference [33]. As seen in Table 3 the Mg 2p main peak energy shifted from 50.1–50.2 eV for the MgO($x \leq 5$)-NiAl catalysts towards lower values for MgO-rich catalysts, MgO(7)-NiAl and MgO(10)-NiAl (49.5 eV and 49.7 eV, respectively). In accordance with He et al. [34], this trend was consistent with an increase of the Mg species film thickness from submonolayer to multilayer coverage. Moreover, the comparison of the Mg 2p peak energy for the MgO(x)-NiAl catalysts with those corresponding to pure MgO and $MgAl_2O_4$ (Table 3) evidenced the increase of $MgAl_2O_4$ phase contribution with MgO loading which was in good agreement with the H_2-TPR data. Besides the main Mg 2p peak the MgO(7)-NiAl and MgO(10)-NiAl spectra revealed the appearance of another peak at a binding energy about 5 eV larger than the main peak. In several studies this additional peak was associated with a growth of tridimensional Mg species which formed islands with a critical size [35].

Table 3 also includes an estimation of Ni/Al and Mg/Al atomic ratios determined by XPS for each catalyst and their comparison with those determined by WDXRF. It was deduced that the Ni/Al XPS ratio remained almost constant for all the samples

(0.22-0.25), but it was lower by 50% with respect to that determined for the bulk analysis (WDXRF). However, the comparison of the Mg/Al bulk ratios (0.06-0.25) with the Mg/Al XPS ratios indicated an apparent enrichment of the near surface with Mg species (0.07 for MgO(2.5)-NiAl, 0.1 for MgO(5)-NiAl, 0.24 for MgO(7)-NiAl and 0.4 for MgO(10)-NiAl).

3.1.5. Transmission electron microscopy (TEM)

The reduced MgO(x)-NiAl samples were investigated by transmission electron microscopy (TEM). Fig. 7 shows the MgO(x)-NiAl micrographs and the corresponding size distribution histograms. The average Ni particle size was estimated from an accumulated frequency including up to 95% of the total population. Table 2 also lists the values of the Ni dispersion and the metallic surface area (S_{Ni}) taking into account the degree of reduction for each catalyst.

Examination of all the micrographs revealed the presence of Ni particles with a quasi spherical shape. Nevertheless, the size distribution seemed to be affected by the MgO addition. For the bare nickel aluminate, MgO(0)-NiAl, the distribution diagram consisted of a broad asymmetric peak, including sizes ranged between 5 and 30 nm, with an average size of 13 nm corresponding to a Ni dispersion of 7% (Table 2). By contrast, a narrower and more symmetric distribution was observed in the case of the MgO(x)-NiAl catalysts thereby indicating an apparent homogeneity of the Ni particle sizes. Furthermore, in agreement with XRD data, smaller Ni particle sizes were deposited in all the MgO-containing samples (11–11.5 nm, D = 8.7–9.4%), thereby suggesting that the addition of magnesia inhibited the sintering of the metallic phase [7,36–38]. Regarding the metallic surface area, it was observed that slightly higher values were obtained for the MgO modified catalysts 14–15 $m^2_{Ni}\,g^{-1}$ compared to the Mg(0)-NiAl catalyst (12 $m^2_{Ni}\,g^{-1}$) (Table 2).

3.1.6. Temperature programmed desorption of CO_2 (CO_2-TPD)

The surface basicity of the reduced MgO(x)-NiAl catalysts was characterised by means of CO_2-TPD techniques. Fig. 8(a) shows the corresponding desorption profiles recorded on the samples after pre-adsorption of CO_2 at 40 °C for 1 h. The amounts of desorbed CO_2 extracted from the integration of the bands centred at three temperature ranges (40–50 °C, 150–350 °C and >350 °C) are reported in Table 4(Fig. 5). Data corresponding to bare alumina are also included for comparison. Generally, at low temperatures the CO_2 desorption peaks are associated with the decomposition of bicarbonates species adsorbed on the weak basic sites [39]. The second temperature range corresponds to a decomposition of bidentate carbonates species which characterise the medium-strength basic sites, while the desorption peaks at high temperatures (>350 °C) are assigned to the decomposition of unidentate carbonates species formed on the strong basic sites.

It was found that the deposition of reduced Ni species onto the alumina surface dramatically increased the total amount as well as the thermal stability of the adsorbed CO_2 (Fig. 8 (a) and Table 4). Indeed, the surface density of CO_2 desorbed from alumina, 0.5 μmol m^{-2}, was much smaller than that determined for MgO(0)-NiAl, 2.7 μmol m^{-2}. However, the total amount of desorbed CO_2 notably decreased in the magnesia doped catalysts. For example, it was about 1.5 μmol m^{-2} for MgO(2.5)-NiAl, 1.9 μmol m^{-2} for MgO(5)-NiAl and 1.2 μmol m^{-2} for MgO(7)-NiAl and MgO(10)-NiAl. This drop in the basic sites density with the MgO content might be related to the structural evolution of Mg species lying on the surface. Indeed, our characterization results pointed out a progressive enrichment of the catalysts with $MgAl_2O_4$ species with MgO loading. In this sense, Cosimo et al. [39] found that in samples with Mg/Al < 1 segregation of bulk $MgAl_2O_4$ spinel occurred and caused a loss in the basic site density.

Table 4 also gives the distribution of the three types of surface basic sites classified according to their strength. When compared to reduced nickel aluminate the distribution appeared to be influenced by the deposition of MgO. It should be highlighted that,

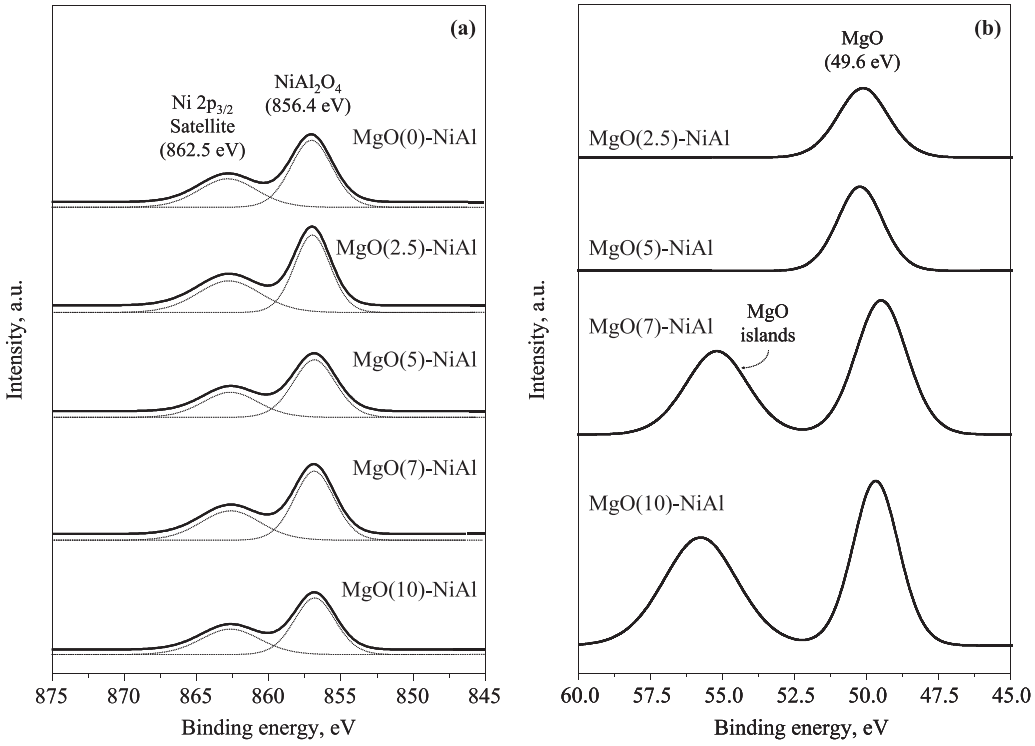

Fig. 6. XPS spectra for the (a) Ni $2p_{3/2}$ and (b) Mg 2p regions of the calcined MgO(x)-NiAl catalysts.

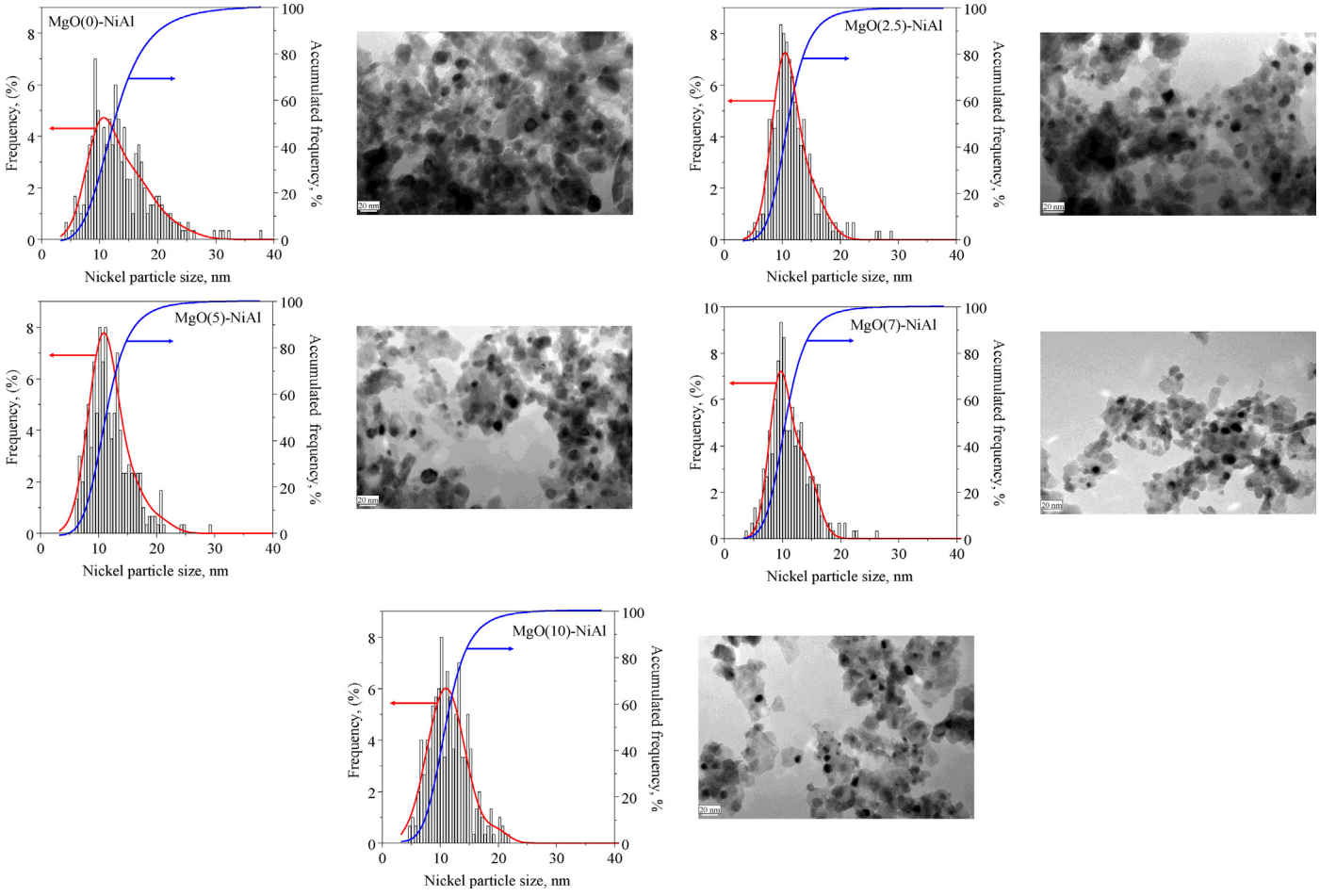

Fig. 7. TEM images and Ni particle sizes distribution of the reduced MgO(x)-NiAl catalysts.

Table 3
XPS study of the MgO(x)-NiAl catalysts.

Catalysts	Main Ni $2p_{3/2}$, eV	FWHM main Ni $2p_{3/2}$, eV	Main Mg 2p, eV	Main O 1s, eV	Ni/Al	Mg/Al	Ni/Al[a]	Mg/Al[a]
MgO(0)-NiAl	855.7	3.5	–	530.6	0.22	0.00	0.50	0.00
MgO(2.5)-NiAl	855.6	3.0	50.1	530.6	0.24	0.07	0.51	0.06
MgO(5)-NiAl	855.2	3.7	50.2	530.3	0.25	0.10	0.50	0.11
MgO(7)-NiAl	855.4	3.4	49.5	530.4	0.22	0.24	0.51	0.17
MgO(10)-NiAl	855.6	3.4	49.7	530.0	0.25	0.40	0.51	0.25
MgO	–	–	50.4	–	–	–	–	–
$MgAl_2O_4$	–	–	49.4	–	–	–	–	–

[a] Determined by WDXRF.

Table 4
Surface basic sites properties as determined by CO_2-TPD study.

Catalysts	Total surface basic sites density, $\mu mol_{CO2}\ m^{-2}$	Weak basic sites, $\mu mol_{CO2}\ m^{-2}$	Medium-strength basic sites, $\mu mol_{CO2}\ m^{-2}$	Strong basic sites, $\mu mol_{CO2}\ m^{-2}$
γ-Al_2O_3	0.5	0.16	0.21	0.13
MgO(0)-NiAl	2.7	0.77	1.04	0.88
MgO(2.5)-NiAl	1.5	0.32	0.08	1.10
MgO(5)-NiAl	1.9	1.00	0.40	0.50
MgO(7)-NiAl	1.2	0.33	0.24	0.64
MgO(10)-NiAl	1.2	0.38	0.18	0.64

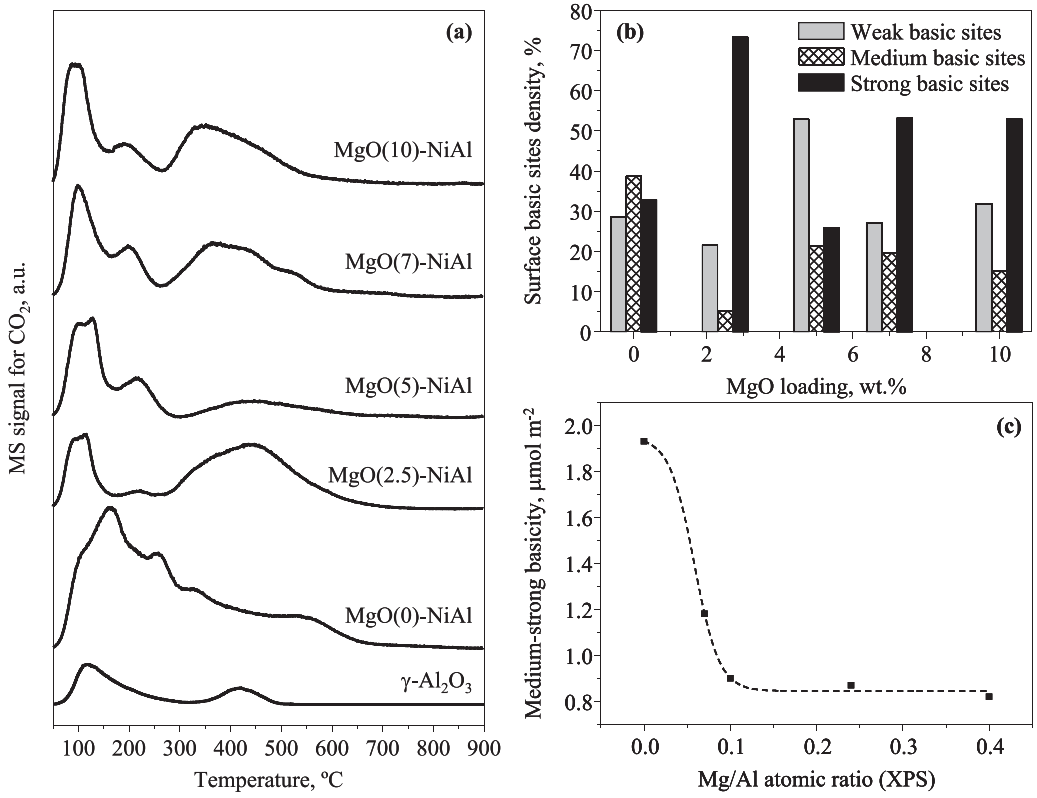

Fig. 8. (a) CO_2-TPD profiles of the reduced MgO(x)-NiAl catalysts, (b) the contribution of each basic sites strength group and (c) the dependence of the density of the medium-strong surface basic sites on the Mg/Al XPS ratios.

among all the analysed samples, this effect was very strong on the MgO(5)-NiAl sample which presented the lowest density of strong basic sites (0.5 $\mu mol\ m^{-2}$) and the highest density of weak basic sites (1 $\mu mol\ m^{-2}$).

To facilitate their comparison the percentage of contribution of each group of basic sites are displayed in Fig. 8(b). For the MgO(0)-NiAl sample the contribution of the weak, medium and strong basic sites was 28.5%, 38.7% and 32.7%, respectively. By contrast, the distribution on the MgO(2.5)-NiAl catalyst evidenced an increase in the fraction of strong basic sites, which accounted for 73.2% of the total amount at the expense of the medium-strength basic sites (5.3%). It was also observed a similar distribution on the MgO-rich samples, MgO(7)-NiAl and MgO(10)-NiAl, thus indicating that the nature of the active sites involved in the adsorption of CO_2 was essentially the same on these two samples. The MgO(5)-NiAl sample presented a distinct behaviour with a major contribution of weak basic sites which represented 52.8% of the total basic sites. This apparent weakening of the surface basic sites could be related

Table 5
Catalytic performance of the MgO(x)-NiAl catalysts in the POM reaction.

Catalysts	X(CH_4), %	Y(H_2)	Y(CO)	Y(CO_2)	H_2/CO	CO/CO_2	Coke, wt.%
Equilibrium	86	0.92	0.81	0.06	2.3	14.6	–
MgO(0)-NiAl	75	0.84	0.65	0.1	2.8	6.2	2.8
MgO(2.5)-NiAl	71	0.76	0.62	0.09	2.7	6.6	7.3
MgO(5)-NiAl	83	0.92	0.75	0.08	2.8	9.6	5.7
MgO(7)-NiAl	78	0.90	0.68	0.1	2.9	7.2	0.7
MgO(10)-NiAl	77	0.87	0.68	0.09	2.8	7.5	6.5
RhAl	86	0.66	0.77	0.09	1.7	8.8	1.7
Reaction conditions: 38,400 cm^3 CH_4 g^{-1} h^{-1}; 10%CH_4/5%O_2/85%N_2; W = 0.125 g; 700 °C; 20 h							
Equilibrium	62	0.90	0.58	0.04	3.1	13.7	–
MgO(0)-NiAl	57	0.41	0.49	0.08	1.7	6.3	43
MgO(2.5)-NiAl	54	0.37	0.44	0.10	1.7	4.6	24
MgO(5)-NiAl	63	0.46	0.56	0.07	1.7	7.8	47
MgO(7)-NiAl	59	0.43	0.51	0.08	1.7	6.7	31
MgO(10)-NiAl	53	0.39	0.43	0.10	1.8	4.3	40
RhAl	61	0.45	0.55	0.07	1.6	8.1	2
MgO(5)-NiAl (75 h)	60	0.45	0.53	0.07	1.7	7.5	68
MgO(7)-NiAl (75 h)	56	0.42	0.47	0.09	1.8	5.4	64
Reaction conditions: 60000 cm^3 CH_4 g^{-1} h^{-1}; 15.6%CH_4/5.9%O_2/78.5%N_2; W = 0.125 g; 700 °C; 20 h/75 h							

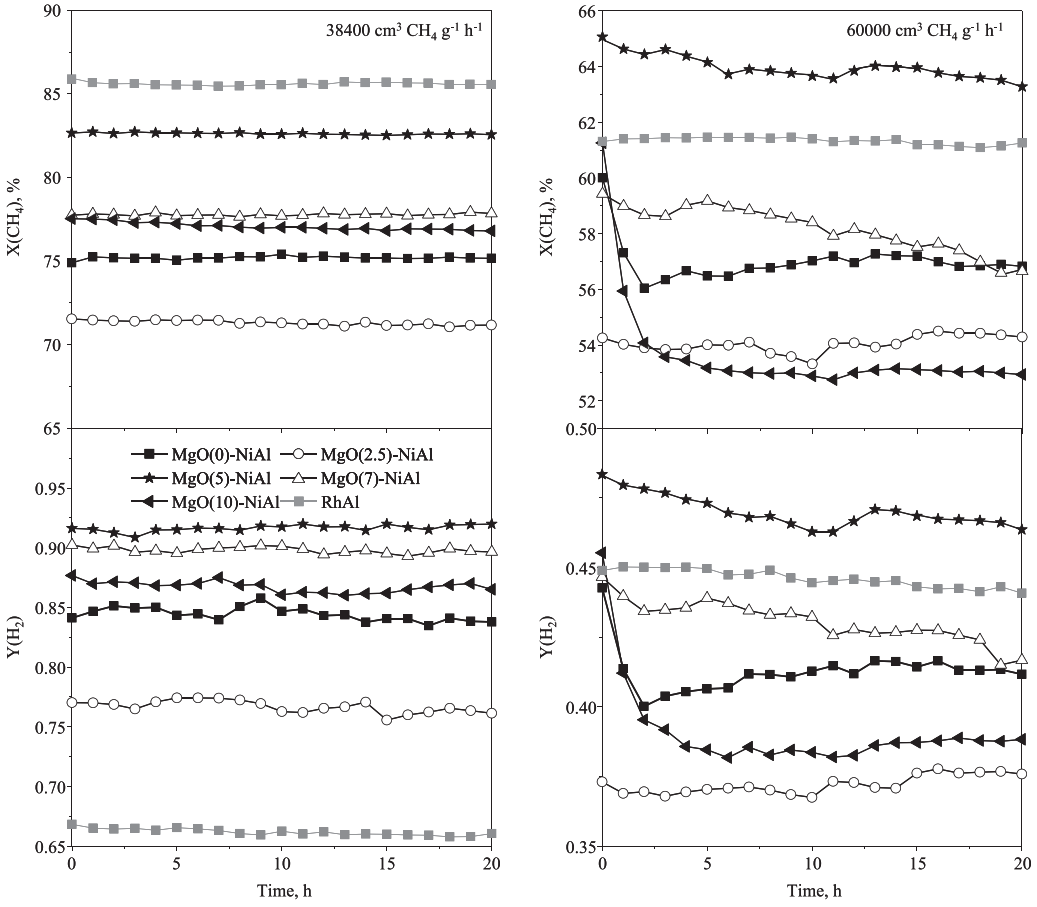

Fig. 9. Catalytic performance in terms of CH_4 conversion and hydrogen yield as a function of time. Reaction conditions: 38400 cm^3 CH_4 g^{-1} h^{-1}; 10%CH_4/5%O_2/85%N_2; W = 0.125 g; 700 °C; 20 h (left) and 60000 cm^3 CH_4 g^{-1} h^{-1}; 15.6%CH_4/5.9%O_2/78.5%N_2; W = 0.125 g; 700 °C; 20 h (right).

to the presence of large amounts of highly dispersed Mg species on the surface.

Due to their relatively higher stability compared to weak basic sites a special attention was paid to the relationship between the amounts of medium and strong basic sites amounts and MgO loading. Fig. 8(c) displays the dependence of the density of basic sites with this strength on the Mg/Al ratios determined by XPS (Table 3). The results showed a significant loss in the surface basicity, respect to MgO(0)-NiAl sample (1.9 μmol m^{-2}), with the abundance of Mg on the near surface up to a value of Mg/Al corresponding to 0.1. For higher Mg/Al ratios the density of medium-strong basic sites remained almost constant, about 0.85–0.9 μmol m^{-2}. Then, the number of the sites involved in the medium-strong basicity was essentially the same on all the over-monolayer samples.

3.2. Catalytic performance in the POM reaction

In our previous study on the activity of Ni catalysts in the partial oxidation of methane an indirect two-step mechanism based on total combustion at lower temeperatures follwed by methane reforming by CO2 and/or steam at high temperatures was verified. Accordingly we found that at lower temperatures (<650 °C) very low CO/CO_2 ratios were obtained thereby suggesting a high combustion activity and a low reforming activity [23]. This poor reforming activity at low temperatures induced, moreover, was related to drastic changes in the Ni oxidation state since inactive NiO was preferentially formed. For this reason, the catalytic tests were carried out at high temperature (700 °C).

3.2.1. Stoichiometric operating conditions (O/C = 1)

Fig. 9 (left) shows the evolution of methane conversion and H_2 yield with time on stream at 700 °C and 38400 cm^3 CH_4 g^{-1} h^{-1} over the reduced MgO(x)-NiAl catalysts. The activity data of a commercial RhAl catalyst was also included for the sake of comparison. As a general behaviour, all the samples exhibited a marked stability in the studied time on stream. Over the MgO-free nickel aluminate sample, MgO(0)-NiAl, both high activity (75%) and H_2 yield (0.84) were found (Table 5). The addition of 2.5% of MgO seemed to provoke a significant decrease in its activity (71%) and the yields of H_2 (0.76) and CO (0.62). However, the addition of MgO concentrations higher than 2.5% induced an improvement of the catalytic performance. For instance, the MgO(5)-NiAl catalyst proved the highest methane conversion (83%), close to that attained by the rhodium catalyst and the thermodynamic equilibrium value (86%), and the highest yields of H_2 and CO (0.92 and 0.75, respectively) whereas it exhibited the lowest yield of CO_2 (0.08). According to their catalytic activity and H_2 yield the MgO(x)-NiAl catalysts followed this trend: MgO(5)-NiAl > MgO(7)-NiAl > MgO(10)-NiAl > MgO(0)-NiAl > MgO(2.5)-NiAl. On the other hand, it should be noted that the MgO(x)-NiAl catalysts demonstrated a relatively good resistance against the coke formation which was lower than 7.3% (Table 5).

The spent catalysts were analysed by XRD in order to determine the nature of deposited carbon and to evaluate the Ni particle sizes. The patterns of the post-run samples (not displayed) showed the appearance of graphitic carbon phase with low intensity signals. On the other hand, the Ni particle sizes estimated by means of Scherrer equation showed generally slight changes (Table 2). Among all the used catalysts the

MgO(2.5)-NiAl catalyst presented the largest particle growth (from 9.5 nm to 13 nm). Table 5 also lists the measured H_2/CO and CO/CO_2 ratios. The H_2/CO ratios over the MgO(x)-NiAl catalysts were in all the cases around 2.7–2.9. These relatively high values (>2) could explain the high stability of the catalysts due to the non-encapsulation of the metal particles by deposited carbon [40]. In our previous study on the performance of the Ni/alumina in the partial oxidation of methane we reported that an increase in active metal dispersion led to higher H_2/CO ratios and an enhanced stability of the catalysts [23]. Accordingly, the similar dispersion of Ni particles, in the 7–9% range, on the MgO(x)-NiAl catalysts could explain the similar obtained H_2/CO ratio values. However, the analysis of the CO/CO_2 ratio values, ranged between 6.2 and 9.6, revealed significant differences among the samples. Generally, the production of CO_2 is related to the occurrence of CO disproportionation and/or methane total oxidation reactions [23]. The gasification of deposited carbon by the produced water (as a product of CH_4 combustion) is one of the reasons that might explain the low carbon deposition detected on the used catalysts.

Since no marked differences were observed in the dispersion of metallic nickel among all the MgO(x)-NiAl catalysts a special attention was devoted to an examination of the influence of structural and chemical properties induced by the Mg species on their catalytic properties. Fig. 10 shows the influence of the strong basic sites density measured by CO_2-TPD on the activity ($X(CH_4)$) and the product distribution ($Y(H_2)$ and CO/CO_2 ratio). The results showed a clear correlation between the surface chemical properties and the catalytic properties of the samples since revealed a decrease in methane conversion and H_2 yields with increasing density of strong basic sites. Furthermore, the dependence trace of CO/CO_2 ratio on the strong basic sites density showed that the reforming activity was governed by the density of strong basic sites. Hence, the sample presenting the lowest strong basic sites density,

MgO(5)-NiAl, exhibited the highest reforming activity.

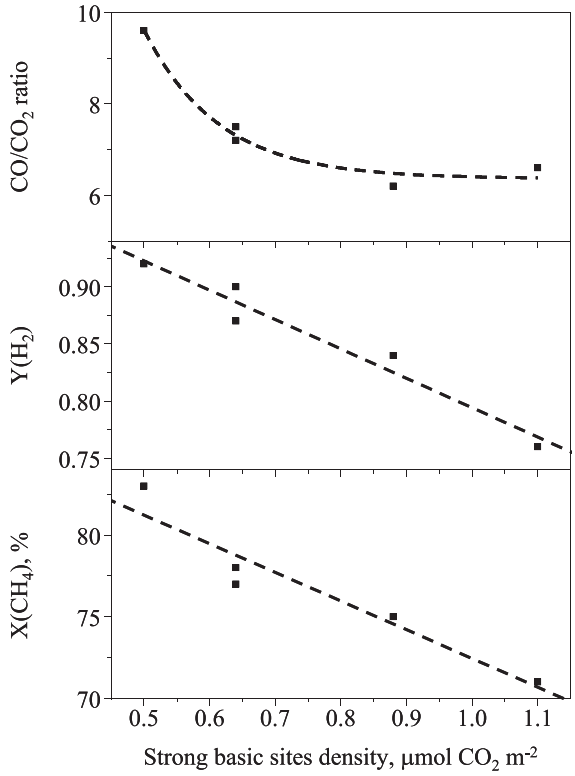

Fig. 10. The influence of the strong basic sites density measured by CO_2-TPD on the activity ($X(CH_4)$,%) and the product distribution ($Y(H_2)$ and CO/CO_2 ratio). Reaction conditions: 38400 cm^3 CH_4 g^{-1} h^{-1}; 10%CH_4/5%O_2/85%N_2; W = 0.125 g; 700 °C; 20 h.

According to Cosimo et al. [39] the strong basic sites that presented high stability predominantly consisted of O^{2-} anions. Moreover, in their study on the mechanism of the POM over a Ni/Al_2O_3 catalyst Jin et al. [41] established that the surface intermediate Ni-C species could react with two types of oxygen species. The first oxygen species named mobile was a product of the activation of oxygen which could react with Ni-C species to produce CO whereas the second species consisted of chemisorbed O^{2-} species which reacted with Ni-C species to produce CO_2. These data could explain the difference observed in the catalytic behaviour of our investigated materials. The observed decrease in the CO/CO_2 ratio with the increase of strong basic density could be associated with the increased amounts of O^{2-} ions which could enhance the formation of CO_2 at the expense of the CO formation.

3.2.2. Non-stoichiometric operating conditions (O/C = 0.75)

In order to examine the stability of the prepared MgO(x)-NiAl samples catalytic runs under more severe conditions were conducted with a higher volume hourly space velocity, namely 60000 cm^3 CH_4 g^{-1} h^{-1}, and a lower O/C molar ratio (from 1 to 0.75) (Fig. 9 (right)). As expected, the selected conditions provoked a decrease in the initial activity of the MgO(x)-NiAl catalysts

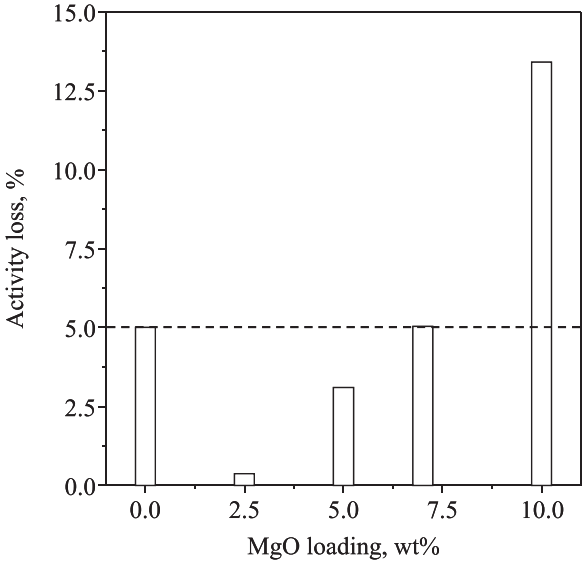

Fig. 11. Dependence of the activity loss (%) in non-stoichiometric conditions (O/C = 0.75) on the MgO loadings.

and an apparent deactivation with time on stream. The amount of deposited carbon was larger than 24 wt.% for all the used catalysts suggesting that the observed deactivation was essentially associated with poisoning of active sites by coke precursors. For instance, the initial methane conversion over the MgO(5)-NiAl catalyst was around 65% (versus 83% obtained with O/C = 1). Even so it kept its superior behaviour compared to the rest of the catalysts. In line with the catalytic results under softer conditions, the initial methane conversion over the studied catalysts seemed to have a similar correlation with the density of strong basic sites densities discussed above. Indeed, it decreased from 65% for the catalyst with the lowest strong sites density, MgO(5)-NiAl, to 54% over the catalyst with the highest strong sites density, MgO(2.5)-NiAl. It should be highlighted that, under non-stoichiometric operating conditions (O/C = 0.75), the MgO addition seemed to improve the resistance against sintering (Table 2). For instance, the Ni particle size on the MgO(0)-NiAl catalyst increased from 9 to 17.5 nm while it did not reach 15 nm on all the Mg catalysts.

Fig. 11 shows the dependence of the activity loss (%), evaluated as the difference between initial conversion and conversion at 20 h divided by the initial conversion, on the MgO loading. For the bare sample, MgO(0)-NiAl, the activity decreased by 5%. The loss of activity upon increasing the MgO content seemed to depend on the differences in the textural properties among the tested catalysts. The addition of an amount of MgO lower than the theoretical monolayer dispersion value improved the stability of the MgO(x)-NiAl catalysts. By contrast, the catalysts with an over-monolayer MgO amounts exhibited a poorer stability when compared to the MgO-free sample. In accordance with our characterisation results it could be concluded that the highly dispersed Mg species enhanced the stability of the MgO(x)-NiAl catalysts whereas an enrichment of the surface with the over-monolayer Mg species accelerated the deactivation of the catalysts.

Given the promising behaviour of MgO(5)-NiAl its performance was evaluated for a considerably more prolonged reaction time interval (75 h) (Fig. 12). For comparison the MgO(7)-NiAl catalyst was also investigated. The results showed that despite the comparable amounts of deposited carbon (64–68 wt.%) and Ni particle sizes (20–21 nm) the MgO(5)-NiAl catalyst maintained its superiority in terms of catalytic performance and stability with respect to the MgO(7)-NiAl catalyst (Table 5). This comparison meant that the catalytic performance differences in the POM reaction were not a

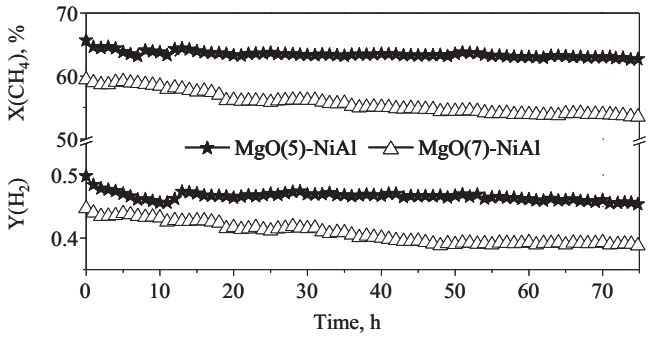

Fig. 12. Stability performance in terms of CH_4 conversion and hydrogen yield over MgO(5)-NiAl and MgO(7)-NiAl catalysts as a function of time. Reaction conditions: 60000 cm^3 CH_4 g^{-1} h^{-1}; 15.6%CH_4/5.9%O_2/78.5%N_2; W = 0.125 g; 700 °C; 75 h.

function of the active nickel state (dispersion and the corresponding deposited carbon amounts). This might point out, however, that the improved structural and chemical properties provided by the highly dispersed Mg species played a key role in the enhancement of the activity and the stability of the MgO(x)-NiAl catalysts in the POM reaction.

4. Conclusions

Bulk nickel aluminate spinel ($NiAl_2O_4$) was synthesised by precipitation and subsequently loaded with varying amounts of MgO (2.5–10 wt.%). The samples in both calcined and reduced catalysts were thoroughly characterised by a wide number of analytical techniques including BET, XRD, H_2-TPR, XPS, TEM and CO_2-TPD. By combining the information obtained from all these studies, a detailed description of the texture, structure, Mg and Ni distribution and chemical properties of the catalysts could be proposed.

The addition of magnesia to the nickel aluminate spinel induced the formation of nickel species with different chemical nature, namely NiO-MgO solid solution, mixed (Ni,Mg)Al_2O_4 spinel and relatively hardly reducible NiO and $NiAl_2O_4$ phases. In contrast to the calcined samples, the formation of $MgAl_2O_4$ was much more pronounced on the reduced samples because of the presence of large amounts of the alumina as a consequence of the reduction of nickel aluminate, which subsequently interact with MgO to form $MgAl_2O_4$ phase. Moreover, on the MgO doped catalysts the metallic nickel particles exhibited a slightly higher resistance to sintering compared to those derived from the bare $NiAl_2O_4$ spinel. In addition, the presence of magnesium species also provoked drastic changes in the number of surface basic sites and their distribution, which could be modulated by modifying the MgO content.

The catalytic behaviour of the reduced samples was investigated in the partial oxidation of methane. The results showed that the modification of $NiAl_2O_4$ by MgO with a concentration higher than 2.5 wt.% clearly enhanced its catalytic performance which was close to that of a commercial Rh catalyst. It was also found that the reforming efficiency (conversion, H_2 yield and stability) could be tuned by controlling the surface strong basic sites density. The MgO(5)-NiAl sample with a magnesium loading close to the theoretical monolayer exhibited the lower density of strong basic sites and the best catalytic performance.

Acknowledgements

The authors wish to thank the financial support for this work provided by the Ministry of Economy and Competitiveness (ENE2013-41187-R), the Basque Government (PRE_2013_2_453, IT657-13) and the University of The Basque Country (UFI 11/39). Technical and human support from SGIker (XRD (A. Larrañaga),

WDXRF (F.J. Sangüesa) and XPS (M.B. Sánchez) and CIC bioGUNE (D. Gil and S. Delgado) is also gratefully acknowledged.

References

[1] M. Momirlan, T.N. Veziroglu, Int. J. Hydrogen Energy 30 (2005) 795–802.
[2] N.Z. Muradov, T.N. Veziroğlu, Int. J. Hydrogen Energy 30 (2005) 225–237.
[3] M.J. Economides, D.A. Wood, J. Nat. Gas Sci. Eng. 1 (2009) 1–13.
[4] S.D. Angeli, G. Monteleone, A. Giaconia, A.A. Lemonidou, Int. J. Hydrogen Energy 39 (2014) 1979–1997.
[5] C. Jiménez-González, Z. Boukha, B. de Rivas, J.R. González-Velasco, J.I. Gutiérrez-Ortiz, R. López-Fonseca, Energy Fuels 28 (2014) 7109–7121.
[6] A.E. York, T. Xiao, M.H. Green, Top. Catal. 22 (2003) 345–358.
[7] H. Özdemir, M.A. Faruk Öksüzömer, M. Ali Gürkaynak, Int. J. Hydrogen Energy 35 (2010) 12147–12160.
[8] J. Zhang, N. Zhao, W. Wei, Y. Sun, Int. J. Hydrogen Energy 35 (2010) 11776–11786.
[9] V.A. Kirillov, Z.A. Fedorova, M.M. Danilova, V.I. Zaikovskii, N.A. Kuzin, V.A. Kuzmin, T.A. Krieger, V.D. Mescheryakov, Appl. Catal. A: Gen. 401 (2011) 170–175.
[10] V.A. Tsipouriari, Z. Zhang, X.E. Verykios, J. Catal. 179 (1998) 283–291.
[11] B. Christian Enger, R. Lødeng, A. Holmen, Appl. Catal. A: Gen. 346 (2008) 1–27.
[12] Y. Song, H. Liu, S. Liu, D. He, Energy Fuels 23 (2009) 1925–1930.
[13] R. López-Fonseca, C. Jiménez-González, B. de Rivas, J.I. Gutiérrez-Ortiz, Appl. Catal. A: Gen. 437–438 (2012) 53–62.
[14] D.V. Cesar, M.A.S. Baldanza, C.A. Henriques, F. Pompeo, G. Santori, J. Múnera, E. Lombardo, M. Schmal, L. Cornaglia, N. Nichio, Int. J. Hydrogen Energy 38 (2013) 5616–5626.
[15] M.C. Campa, G. Ferraris, D. Gazzoli, I. Pettiti, D. Pietrogiacomi, Appl. Catal. B: Environ. 142–143 (2013) 423–431.
[16] Y. Kobayashi, J. Horiguchi, S. Kobayashi, Y. Yamazaki, K. Omata, D. Nagao, M. Konno, M. Yamada, Appl. Catal. A: Gen. 395 (2011) 129–137.
[17] L.D. Vella, S. Specchia, Catal. Today 176 (2011) 340–346.
[18] Y. Kathiraser, W. Thitsartarn, K. Sutthiumporn, S. Kawi, J. Phys. Chem. C 117 (2013) 8120–8130.
[19] N.F.P. Ribeiro, R.C.R. Neto, S.F. Moya, M.M.V.M. Souza, M. Schmal, Int. J. Hydrogen Energy 35 (2010) 11725–11732.
[20] B.S. Liu, C.T. Au, Appl. Catal. A: Gen. 244 (2003) 181–195.
[21] R. Pereñíguez, V.M. González-DelaCruz, J.P. Holgado, A. Caballero, Appl. Catal. A: Gen. 93 (2010) 346–353.
[22] T.H. Nguyen, A. Łamacz, P. Beaunier, S. Czajkowska, M. Domański, A. Krztoń, T. Van Le, G. Djéga-Mariadassou, Appl. Catal. B: Environ. 152–153 (2014) 360–369.
[23] Z. Boukha, C. Jiménez-González, B. de Rivas, J.R. González-Velasco, J.I. Gutiérrez-Ortiz, R. López-Fonseca, Appl. Catal. B: Environ. 158–159 (2014) 190–201.
[24] M.J. Holgado, V. Rives, M.S. San Roman, Appl. Catal. A: Gen. 214 (2001) 219–228.
[25] L.J.I. Coleman, W. Epling, R.R. Hudgins, E. Croiset, Appl. Catal. A: Gen. 363 (2009) 52–63.
[26] W. Gac, Appl. Surf. Sci. 257 (2011) 2875–2880.
[27] H.S.A. de Sousa, A.N. da Silva, A.J.R. Castro, A. Campos, J.M. Filho, A.C. Oliveira, Int. J. Hydrogen Energy 37 (2012) 12281–12291.
[28] Z. Jiang, J. Su, M.O. Jones, H. Shi, T. Xiao, P.P. Edwards, Energy Fuels. 23 (2009) 1634–1639.
[29] G. Li, L. Hu, J.M. Hill, Appl. Catal. A: Gen. 301 (2006) 16–24.
[30] A. Penkova, L. Bobadilla, S. Ivanova, M.I. Domínguez, F. Romero-Sarria, A.C. Roger, M.A. Centeno, J.A. Odriozola, Appl. Catal. A: Gen. 392 (2011) 184–191.
[31] K.T. Jacob, K.P. Jayadevan, Y. Waseda, J. Am. Ceram. Soc. 81 (1998) 209–212.
[32] H. Özdemir, M.A.F. Öksüzömer, M.A. Gürkaynak, Fuel 116 (2014) 63–70.
[33] S. Ardizzone, C.L. Bianchi, M. Fadoni, B. Vercelli, Appl. Surf. Sci. 119 (1997) 253–259.
[34] J.- He, J.S. Corneille, D.W. Goodman, Appl. Surf. Sci. 72 (1993) 335–340.
[35] M. Kurth, P.C.J. Graat, E.J. Mittemeijer, Appl. Surf. Sci. 220 (2003) 60–78.
[36] Y.H. Hu, E. Ruckenstein, Catal. Rev. Sci. Eng. 44 (2002) 423–453.
[37] M. García-Diéguez, C. Herrera, M.Á. Larrubia, L.J. Alemany, Catal. Today 197 (2012) 50–57.
[38] J. Min, Y. Lee, H. Park, C. Zhang, K. Jun, J. Ind. Eng. Chem. 26 (2015) 375–383.
[39] J.I. Di Cosimo, M. Díez, E. Iglesia, C.R. Apesteguía, J. Catal. (1998) 499–510.
[40] C.H. Bartholomew, Appl. Catal. A: Gen. 212 (2001) 17–60.
[41] R. Jin, Y. Chen, W. Li, W. Cui, Y. Ji, C. Yu, Y. Jiang, Appl. Catal. A: Gen. 201 (2000) 71–80.